Hydrology and
Earth System
Sciences

Vegetation optimality explains the convergence of catchments on the Budyko curve

Remko C. Nijzink and Stanislaus J. Schymanski

Catchment and Ecohydrology Group (CAT), Environmental Research and Innovation (ERIN),
Luxembourg Institute of Science and Technology (LIST), Belvaux, Luxembourg

Correspondence: Remko C. Nijzink (remko_nijzink@live.nl)

Abstract. The Budyko framework puts the long-term mean annual evapotranspiration (ET) of a catchment in relation to its maximum possible value determined by the conservation of mass (ET cannot exceed mean annual precipitation) and energy (ET can not exceed mean annual net radiation) in the absence of significant storage contributions. Most catchments plot relatively close to this physical limit, which allowed the development of an empirical equation (often referred to as the Budyko curve) for estimating mean annual evaporation and runoff from observed net radiation and precipitation. Parametric forms of the curve often use a shape parameter, n, that is seen as a catchment characteristic. However, a satisfying explanation for the convergence and self-organization of catchments around such an empirical curve is still lacking. In this study, we explore if vegetation optimality can explain the convergence of catchments along a Budyko curve and in how far can n be seen as a catchment characteristic.

The Vegetation Optimality Model (VOM) optimizes vegetation properties and behavior (e.g., rooting depths, vegetation cover, stomatal control) to maximize the difference between the total carbon taken up from the atmosphere and the carbon used for maintenance of plant tissues involved in its uptake, i.e., the long-term net carbon profit (NCP). This optimization is entirely independent of observed ET and hence the VOM does not require calibration for predicting ET. In a first step, the VOM was fully optimized for the observed atmospheric forcing at five flux tower sites along the North Australian Tropical Transect, as well as 36 additional locations near the transect and six Australian catchments. In addition, the VOM was run without vegetation for all sites, meaning that all precipitation was partitioned into soil evapora-

tion and runoff. For comparison, three conceptual hydrological models (TUWmodel, GR4J, and FLEX) were calibrated for the Australian catchments using the observed precipitation and runoff. Subsequently, we emulated step changes in climate by multiplying precipitation (P) by factors ranging between 0.2 and 2 before running the VOM and hydrological models without changing the vegetation properties or model parameters, emulating invariant catchment characteristics under a changed climate. In a last step, the VOM was re-optimized for the different P amounts, allowing vegetation to adapt to the new situation. Eventually, Budyko curves were fit by adapting the parameter n to the model results. This was carried out for both multiple sites simultaneously and for each individual study site, thereby assuming that n is a site-specific characteristic.

The optimized VOM runs tracked relatively close to a Budyko curve with a realistic n value and close to observations, whereas the runs without vegetation led to significantly lower evaporative fractions and unrealistically low n values compared with literature. When fitting n to individual catchments, changes in P led to changes in n (increasing n for decreasing P) in all model runs (including the three conceptual models) except if the VOM was re-optimized for each change in P, which brought the value of n back close to its value for the unperturbed P in each catchment. For the re-optimized VOM runs, the variation in n between catchments was greater than within each catchment in response to multiplications of P with a factor 0.2 to 2.

These findings suggest that optimality may explain the self-organization of catchments in Budyko space, and that the accompanying parameter n does not remain constant for constant catchment and vegetation conditions as hypothesized

in the literature, but in fact emerges through the adaptation of vegetation to climatic conditions in a given hydrological setting. Moreover, the results suggest that n might initially increase in response to suddenly reduced P, and only slowly returns to its original, catchment-specific value, as vegetation re-adjusts to the new climate over decades and centuries. This may constitute a new basis for the evaluation and prediction of catchment responses to climatic shifts.

1 Introduction

Conservation of mass is a fundamental physical law that is commonly invoked in catchment hydrology. Essentially, it means that the net exchange of water across catchment boundaries (due to precipitation (P), evapotranspiration (E_T), and discharge (Q)) equals the change in catchment water storage over time. Another fundamental physical law is conservation of energy, which puts an upper bound on how much water can leave the catchment by evapotranspiration, as the phase change from liquid to gaseous water requires a large amount of energy, which is mainly supplied by the sun. When considering long timescales (e.g., decades), a potential change in storage becomes tiny compared to the cumulative fluxes, which allows the prediction that the total evapotranspiration (E_T) of a catchment cannot exceed the integrated amount of precipitation over the same time period. Another limit is defined by the integrated amount of energy available for E_T ("potential evaporation", E_p), which the total evapotranspiration (E_T) cannot exceed either. Already in the early 1900s, scientists found out that E_T estimated from the difference between long-term precipitation and runoff ($E_T = P - Q$) tracks relatively close to these limits in large catchments, and they proposed empirical equations to predict mean annual E_T and runoff from observed net radiation and precipitation (Ol'Dekop, 1911; Schreiber, 1904). Budyko (1974) combined these empirical equations to what we call here the Budyko curve and formulated a framework with a catchment dryness index E_p/P as independent variable and the evapotranspired fraction of precipitation (E_T/P) as dependent variable. Note that the framework can alternatively be presented with a wetness index P/E_p as independent variable (Yang et al., 2008; Roderick and Farquhar, 2011; Nijzink and Schymanski, 2022b), as introduced by Pike (1964).

The Budyko framework has been widely used in catchment science and has proven to be a powerful tool in order to assess the water balance in relation to its physical boundaries. Early focus fell on explaining the spread around the empirical curve. For example, Budyko (1974) argued that downwards deviations from the curve are bigger where seasonal signals of potential evaporation and rainfall were out of phase, which was later confirmed by others (Yokoo et al., 2008; Potter et al., 2005). It was also shown that variations

in soil moisture storage capacity (e.g., Milly, 1994; Woods, 2003), land cover (Oudin et al., 2008), and vegetation (Donohue et al., 2007) are able to explain deviations from the curve.

As more catchments were analyzed in the Budyko framework, more systematic deviations from the original Budyko curve were discovered, motivating more flexible formulations with an additional parameter to adjust the shape of the curve (Fu, 1981; Choudhury, 1999; Zhang et al., 2001, 2004). Yang et al. (2008) demonstrated that the two widespread flexible parameter formulations of Fu (1981) and Choudhury (1999) (also attributed to Mezentsev, 1955) are approximately equivalent if their shape parameters followed a certain linear relationship to each other. Therefore, we will use the formulation by Choudhury (1999) and refer to the parameter as n here, regardless of its name in the different publications cited hereafter. Interestingly, the meaning of the additional parameters were explained in different ways by different authors. For example, Zhang et al. (2001) called n the plant available water coefficient, while Ning et al. (2017) fitted separate values of n each year and related these values to annual measures of seasonality and vegetation cover. Donohue et al. (2012) used a multi-variate approach to explain variations in n by local rooting depths, storm depths, and soil water storage capacities. Similarly, Roderick and Farquhar (2011) argued that this parameter should be considered a result of all local conditions combined (except for climate). Specifically, in their analysis of runoff sensitivity to perturbations in P and E_p, they held n constant, followed by a separate sensitivity analysis to perturbations in n, arguing that n would only change over longer timescales, e.g., due to a change in vegetation cover.

While explanations for deviations from the Budyko curve (e.g., Roderick and Farquhar, 2011; Donohue et al., 2012; Ning et al., 2017) and the practical use of the Budyko framework (e.g., Nijzink et al., 2018; Hulsman et al., 2018; Mianabadi et al., 2019) are being explored intensively to this day, less attention has been put on explaining why catchments converge on a curve in Budyko space at all, instead of randomly falling somewhere in the envelope determined by the conservation of mass and energy. Optimality theory could provide a promising avenue to explain this convergence, as it allows selecting the most likely states of a system from the range of possible states. Wang et al. (2015) and Westhoff et al. (2016) used thermodynamic optimality principles (maximum entropy production and maximum power, respectively) to produce curves resembling the Budyko curve, but they did not explain the role of vegetation for the shape of the curve, as suggested by many authors (e.g., Roderick and Farquhar, 2011; Donohue et al., 2007; Oudin et al., 2008; Yang et al., 2009; Williams et al., 2012). Here we investigate if vegetation optimality explains the convergence of catchments on the Budyko curve. Vegetation optimality proposes that vegetation self-optimizes to maximize its long-term net carbon profit (NCP), which is the difference between carbon taken up during photosynthesis and carbon invested in plant

organs involved in carbon and water uptake and transport. The principle was implemented by Schymanski et al. (2009) in the Vegetation Optimality Model (VOM), which couples a vegetation and water balance model, and was shown to reproduce observed carbon and water fluxes at several tropical savanna sites in Australia (Schymanski et al., 2009; Nijzink et al., 2022a) and explain general trends in vegetation responses to elevated atmospheric CO_2 concentrations (Schymanski et al., 2015). The model distinguishes between slowly optimizing vegetation properties, such as water-use strategies, tree cover, and rooting depths, and quickly optimizing vegetation properties, such as photosynthetic capacities, vertical root distributions, grass cover, and stomatal conductances. The former are held constant over decades, while the latter vary at a seasonal or even hourly scale. This enables the distinction between day-to-day responses of vegetation to environmental drivers, and the slow responses (e.g., tree cover, species composition) assumed to result in changing n values (Roderick and Farquhar, 2011).

Based on the above considerations, we formulated the following hypotheses.

H1   Model simulations based on vegetation optimality lead to a better reproduction of the empirical Budyko curve than model simulations without self-optimized vegetation.

H2   The empirical parameter n stays constant as climate changes, as long as vegetation cover and rooting depths stay constant.

H3   Changes in n values are a result of slowly varying long-term vegetation properties.

2   Methodology

In order to address the hypotheses, three hydrological models and the VOM were applied to several sites in Australia. All the analyses and model runs were carried out with an open science approach by using the platform Renku (https://renkulab.io/, last access: 10 February 2022) that tracks all steps in the scientific process. The resulting workflows including code and data can be found online (Nijzink and Schymanski, 2022a, https://renkulab.io/projects/remko.nijzink/budyko, last access: 1 December 2022).

2.1   Budyko formulations

In this study, we start from Eq. (1) in Roderick and Farquhar (2011) (which is equivalent to Eq. 3 in Choudhury, 1999 and was traced back to Mezentsev, 1955 by Yang et al., 2008):

$$\overline{E_a} = \frac{\overline{E_p}\,\overline{P}}{\left(\overline{P}^n + \overline{E_p}^n\right)^{1/n}}, \tag{1}$$

with $\overline{E_p}$ the mean annual potential evaporation, $\overline{E_a}$ the mean annual evaporation, $\overline{P}$ the mean annual precipitation, and n a shape factor, assumed to represent catchment characteristics (e.g., vegetation, soils). To express the ratio $\overline{E_a}/\overline{P}$ as a function of $\overline{E_p}/\overline{P}$ (see also Supplement S5), both sides of Eq. (1) were divided by $\overline{P}$ and the resulting nominator and denominator on the right hand side were again divided by $\overline{P}$. Following Budyko (1974), $\overline{E_p}$ was expressed as a function of mean annual net radiation ($\lambda\overline{E_p} = \overline{R_n}$), and all fluxes were transformed in terms of energy by multiplying by the latent heat of vaporization λ:

$$\frac{\lambda\overline{E_a}}{\lambda\overline{P}} = \frac{\overline{R_n}}{\lambda\overline{P}}\left(\left(\frac{\overline{R_n}}{\lambda\overline{P}}\right)^n + 1\right)^{-1/n}. \tag{2}$$

In a similar way, Eq. (1) can be transformed into an equation with the fraction of $\lambda\overline{P}/\overline{R_n}$ as the independent variable (see also Supplement S5), by first dividing both sides of Eq. (1) by $\overline{E_p}$, followed by a division of the nominator and denominator of the right hand side by $\overline{E_p}$ and a conversion to energetic units:

$$\frac{\lambda\overline{E_a}}{\overline{R_n}} = \frac{\lambda\overline{P}}{\overline{R_n}}\left(\left(\frac{\lambda\overline{P}}{\overline{R_n}}\right)^n + 1\right)^{-1/n}. \tag{3}$$

For fits to single data points (i.e., one catchment/study site), the equations were solved analytically using open-source software (sympy, https://www.sympy.org/, last access: 10 February 2022, essm https://pypi.org/project/essm/, last access: 10 February 2022). The exponent n in Eqs. (2) and (3) was fitted to data of multiple catchments with a non-linear least squares fit based on the Levenberg–Marquardt algorithm (python scipy.optimize.curve_fit, https://docs.scipy.org/doc/scipy/reference/generated/scipy.optimize.curve_fit.html, last access: 10 February 2022, Levenberg, 1944). The mean square error (MSE) was used in order to assess the goodness of fit:

$$\text{MSE} = \frac{1}{m}\sum_{i=1}^{m}\left(Y_i - \overline{Y}_i\right)^2, \tag{4}$$

with m the number of observations, Y_i an individual observation, and $\overline{Y}_i$ the predicted value.

2.2   Study sites

In order to capture a variation of climates, the study focuses on several sites along a precipitation gradient in Australia. The study sites include flux tower sites where the VOM has been tested previously (Nijzink et al., 2022b, a) as well as several larger catchments. An additional analysis based on a selection of 357 catchments of the CAMELS dataset (Addor et al., 2017; Newman et al., 2015) is presented in Supplement S3, Fig. S3.8–S3.11.

2.2.1 North Australian Tropical Transect

The Vegetation Optimality Model (VOM, see Sect. 2.3) was set up for five flux tower sites that are located between 12.5 and 22.5° S along the North Australian Tropical Transect (NATT, Hutley et al., 2011). The precipitation decreases from 1700 to 500 mm yr^{-1} from north to south along the transect, over a distance of approximately 1000 km. The five sites used in this study are summarized in Table 1 and the geographical locations are shown in Fig. 1, see also Nijzink et al. (2022b) and Nijzink et al. (2022a). A more detailed description of the sites can be found in Hutley et al. (2011). In addition to the flux tower sites, 36 locations along the transect were used (see also Fig. 1), which were all located between 12.5 and 17.5° S, and 131.0° E and 133.5° S, with a distance between the locations of 0.5°.

The soil parameterization of the VOM is based on data of the Soil and Landscape Grid of Australia (Viscarra Rossel et al., 2014a, b, c), in addition to specific site descriptions provided by Hutley et al. (2011) and Whitley et al. (2016). For a description of the soil profiles, see also Supplement S8 of Nijzink et al. (2022a). Meteorological data from the Australian SILO Data Drill (Jeffrey et al., 2001) were used to run the model and consisted of time series of daily maximum and minimum temperatures, shortwave radiation, precipitation, vapor pressure, and atmospheric pressure. The Mauna Loa CO_2 records (Keeling et al., 2005) provided time series of atmospheric CO_2 concentrations.

2.2.2 Australian catchments

The NATT sites described above were not part of any hydrologically gauged catchments, and therefore we selected an additional six catchments with runoff data, which were close to the NATT sites and had similar climates. This allowed to compare VOM results with the results of three relatively simple conceptual hydrological models (FLEX, TUW-model, and GR4J, see Sect. 2.4), which require runoff data for calibration. These catchments were also previously used by Zhang et al. (2004) in their Budyko analysis. See Table 2 for details of these catchments and Fig. 1 for their locations. Meteorological data were again taken from the Australian SILO Data Drill (Jeffrey et al., 2001), from which time series of potential evaporation (FAO, Penman–Monteith formula, Allen et al., 1998), precipitation, and daily maximum and minimum temperatures were used to run the hydrological models. The VOM used again time series of the SILO data drill of daily maximum and minimum temperatures, shortwave radiation, precipitation, vapor pressure, and atmospheric pressure. The Mauna Loa CO_2 records (Keeling et al., 2005) again provided time series of atmospheric CO_2 concentrations for the VOM simulations.

2.3 Vegetation Optimality Model

The Vegetation Optimality Model (VOM, Schymanski et al., 2009, 2015; Nijzink et al., 2022b) is a combined water and vegetation model that optimizes vegetation properties, such as rooting depths and foliage cover, in order to maximize the net carbon profit (NCP), defined here as the difference between carbon taken up by photosynthesis and the carbon invested into maintenance of leaves, roots, and water transport tissues. The model code and documentation can be found online (https://github.com/schymans/VOM, last access: 10 February 2022, https://vom.readthedocs.io, last access: 10 February 2022) and a more detailed description can be found in Schymanski et al. (2009, 2015), Nijzink et al. (2022b) as well as Supplement S6. VOM version v0.6 (https://github.com/schymans/VOM/tree/v0.6, last access: 4 March 2022) was used in this study.

2.3.1 Vegetation model

Vegetation is schematized in the VOM as two big leaves, with one leaf representing the perennial vegetation (trees) and one leaf representing the annual grasses. The photosynthesis of these leaves is calculated based on a simplified canopy–gas exchange model for C3 plants (Schymanski et al., 2007), based on von Caemmerer (2000), which uses irradiance, atmospheric CO_2 concentration, temperature, photosynthetic capacity, and stomatal conductance:

$$
\begin{aligned}
A_g = \frac{1}{8}\bigg(& 4C_aG_s + 8\Gamma_*G_s \\
& + \big((J_e - 4R_l - 4G_s(C_a - 2\Gamma_*))^2 \\
& + 16G_s\big(8C_aG_s + J_e + 8R_l\big)\Gamma_*\big)^{\frac{1}{2}}\bigg),
\end{aligned}
\tag{5}
$$

with J_e the electron transport rate (mol m^{-2} s^{-1}), G_s stomatal conductance (mol m^{-2} s^{-1}), R_l leaf respiration (mol m^{-2} s^{-1}), C_a the mole fraction of CO_2 in the air, and Γ_* the CO_2 compensation point (mol CO_2 mol^{-1} air).

Stomatal conductance and observed water vapor deficit are used to compute transpiration rates:

$$
E_t = a \cdot G_s \cdot (W_l - W_a),
\tag{6}
$$

with a the ratio of diffusivities of water vapor and CO_2 in air, G_s stomatal conductance (mol m^{-2} s^{-1}), W_l the mole fraction of water vapor in air inside the leaf, and W_a the mole fraction of water vapor in the atmosphere. At the same time, the transpiration can be limited by the root water uptake, which is driven by the water potential difference between the plant and each soil layer, following an electrical circuit analogy (Schymanski et al., 2008).

In order to calculate the NCP (i.e., the objective function), the VOM subtracts respiration of roots and leaves (R_r) as
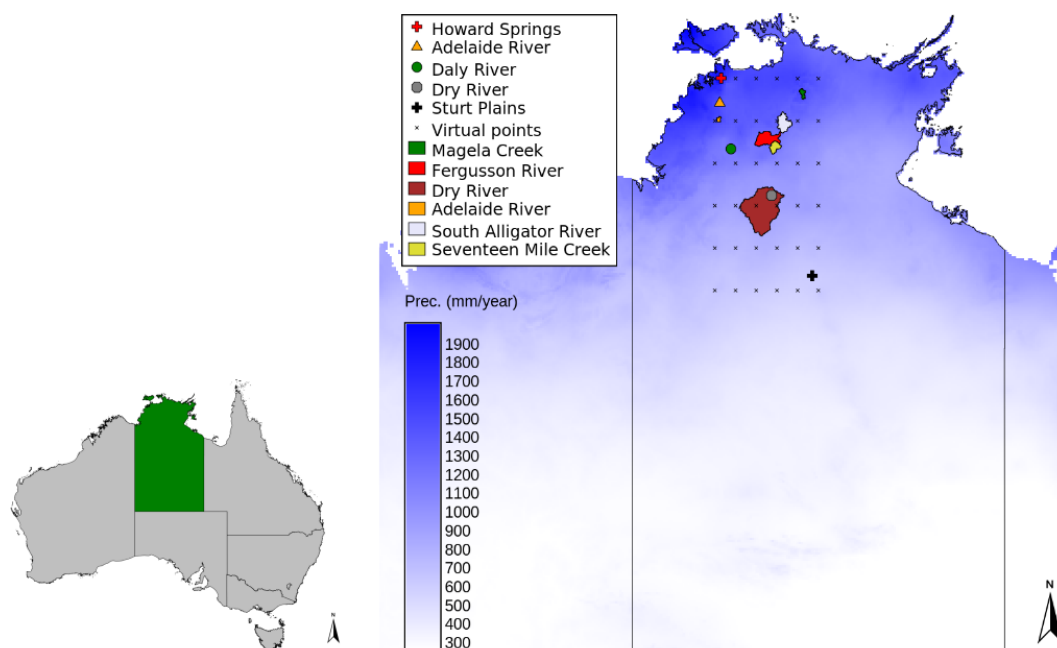
Figure 1. Catchments (polygons) and flux tower sites along the North Australian Tropical Transect (symbols), with additional locations shown as crosses. The mean annual precipitation is indicated by the blue color scale.

Table 1. Characteristics of the study sites along the North Australian Tropical Transect, vegetation data from Hutley et al. (2011) and Whitley et al. (2016), with *Eucalyptus* (Eu.), *Erythrophleum* (Er.), *Terminalia* (Te.), *Corymbia* (Co.), *Planchonia* (Pl.), *Themeda* (Th.), *Hetropogan* (He.), and *Chrysopogon* (Ch.). Meteorological data are taken from the SILO data drill (Jeffrey et al., 2001) for the model periods of 1 January 1980 until 31 December 2017, including the Food and Agriculture Organization of the United Nations (FAO) Penman–Monteith potential evaporation (Allen et al., 1998). Aridity is defined as the ratio of net radiation to precipitation (multiplied by the latent heat of vaporization λ), $R_n/(\lambda P)$. Tree cover is determined as the minimum value of the mean monthly projective cover based on remotely sensed observations of the fraction of photosynthetically active radiation (fPAR Donohue et al., 2008). The maximum grass cover was found by subtracting the tree cover from the remotely sensed projective cover.

Study site	Howard Springs	Adelaide River	Daly River	Dry River	Sturt Plains
FLUXNET ID	AU-How	AU-Ade	AU-DaS	AU-Dry	AU-Stp
Coordinates	12.49° S	13.08° S	14.16° S	15.26° S	17.15° S
	131.35° E	131.12° E	131.39° E	132.37° E	133.35° E
Prec. (mm yr^{-1})	1747	1497	1166	898	616
Pot. evap. (mm yr^{-1})	1763	1802	1896	1948	2082
Aridity. (–)	1.03	1.18	1.48	1.87	2.70
Net rad. (MJ m^{-2} yr^{-1})	4392	4313	4215	4105	4079
Mean max. temp. [°C]	37.5	38.8	40.6	41.1	43.0
Mean min. temp. [°C]	27.4	26.6	26.9	27.7	28.1
Tree cover (%)	39.8	20.8	37.5	26.6	7.4
Max. grass cover (%)	44.3	59.2	42.5	49.4	57.6
Species					
Overstorey	*Eu. miniata*	*Eu. tectifica*	*Te. grandiflora*	*Eu. tetrodonta*	–
	Eu. tetrodonta	*Co. latifolia*	*Eu. tetrodonta*	*Co. terminalis*	
	Er. chlorostachys	*Pl. careya*	*Co. latifolia*	*Eu. dichromophloia*	
Understorey	*Sorghum spp.*	*Sorghum spp.*	*Sorghum spp.*	*Sorghum intrans*	*Astrebla spp.*
	He. triticeus	*Ch. fallax*	*He. triticeus*	*Th. Tiandra*	
				Ch. fallax	

Table 2. Characteristics of the six Australian catchments.

Study site	Area (km^2)	Aridity (–)	Prec. (mm yr^{-1})	Pot. evap. (mm yr^{-1})	Discharge (mm yr^{-1})	Data availability
Adelaide River	115.0	1.17	1469	1715	282	27 August 1981–13 July 2020
Dry River	8235.9	2.24	848	1895	27	1 January 1980–13 July 2020
Fergusson River	1686.1	1.51	1160	1750	327	1 January 1980–19 April 2020
Magela Creek	265.5	1.08	1457	1580	695	1 January 1980–2 November 2006
Seventeen Mile Creek	602.2	1.55	1133	1756	363	1 January 1980–13 July 2020
South Alligator River	1218.0	1.31	1267	1663	505	1 January 1980–8 June 2010

well as the maintenance and turnover carbon costs of foliage (R_f) from the photosynthetic carbon uptake. In addition, carbon costs for the water transport system (R_v) are represented as a function of rooting depth and projected vegetation cover and also subtracted from the carbon uptake:

$$\mathrm{NCP} = \int \big(A_g(t) - R_f(t) - R_r(t) - R_v(t)\big)\,\mathrm{d}t, \qquad (7)$$

with t representing the time step.

Each optimized vegetation property thus incurs both a benefit (e.g., increasing light or water supply for photosynthesis) and a cost (construction/maintenance), defining the NCP, but they are optimized at different timescales. Rooting depths of the perennial trees and seasonal grasses ($y_{r,p}$ and $y_{r,s}$, respectively), the foliage projected cover of the perennial vegetation ($M_{A,p}$), and two parameters defining the water use strategy of each big leaf are assumed to be constant during the simulation period of 37 years and optimized to maximize the NCP over the entire period. In contrast, seasonal vegetation cover and photosynthetic capacities of the seasonal and perennial vegetation are adjusted incrementally from day to day based on the daily NCP on the previous day. At the same time, as soil moisture gets depleted, soil water potential declines, and if canopy water demand cannot be matched by root water uptake, the model reduces stomatal conductance (i.e., G_s in the equations above) below its optimized value and increases root surface area.

2.3.2 Water balance model

The water balance part of the model (see also Schymanski et al., 2008, 2015) was set up as described by Nijzink et al. (2022b). Briefly, the VOM schematizes the soil as a block with layers of 0.2 m thickness and a total thickness of 30 m (i.e., 150 layers). Vertical flow between the layers is possible down to the last impermeable layer, whereas lateral drainage can occur from the saturated layers. The VOM was parameterized in a way to resemble freely draining conditions, which was done due to the absence of detailed knowledge about the hydrology of the sites. Precipitation can either infiltrate, directly run off as surface runoff, or evaporate right away as soil evaporation, depending on the saturation of the

top soil layer. Afterwards, water can either percolate further down towards more saturated layers or be taken up by roots for transpiration. A drainage flux sets in as soon as the water table exceeds a prescribed drainage level, which is set here to 25 m below the surface. In this way, the groundwater table was kept well outside the reach of roots, i.e., resembling free drainage conditions.

2.3.3 Optimization

The shuffled complex evolution algorithm (SCE, Duan et al., 1994) was used to optimize the long-term parameters in the VOM for the full simulation period of 37 years (1 January 1980 until 31 December 2017). The number of initial complexes was set to 10, after which the algorithm performs a local optimization within each complex. Afterwards, the complexes are mixed, aiming to find the global optimum. For the day-to-day optimization of the variable vegetation properties, the model was run with the actual and a higher and lower value of each property for each day, and the properties were adjusted at the end of each day to the combination that would have led to the maximum daily NCP.

2.4 Conceptual hydrological models

Three relatively simple conceptual hydrological models were selected in order to compare with the more complex VOM. These were selected in order to represent a commonly used model (the TUWmodel, a version of the HBV model), a slightly more complex model with more calibration parameters (FLEX), and a model with a very parsimonious number of parameters (the GR4J model). Details about the models can be found in Supplement S6.

2.4.1 TUWmodel

The TUWmodel (https://cran.r-project.org/web/packages/TUWmodel/, last access: 10 February 2022, Parajka et al., 2007) is a version of the widely used Hydrologiska Byråns Vattenbalansavdelning (HBV) model (Bergström, 1976) that consists of a set of reservoirs in series. The effective precipitation is determined by a snow module, after which it enters a soil moisture module. The current soil moisture state deter-

mines how much of the effective precipitation will infiltrate and how much will go to a fast reservoir for runoff.

In this model, vegetation is not modeled explicitly. However, the influence of vegetation can be noted from the total evaporation rate (including transpiration) that depends on the fractional filling of the soil moisture reservoir as well as the potential evaporation:

$$E_T = \begin{cases} \frac{S_m}{LP} \cdot E_p, & \text{if } S_m < \text{LPrat} \cdot \text{FC} \\ E_p, & \text{if } S_m >= \text{LP} \end{cases}, \qquad (8)$$

with S_m the soil moisture state [mm], LPrat a constant calibration parameter reflecting the soil moisture threshold after which evaporation occurs at a potential rate [–], and FC the field capacity [mm].

Furthermore, the fast reservoir has an overflow outlet that accounts for the fast overland flow component and a normal reservoir outlet. From this fast reservoir, water can also percolate further down to a slow reservoir that represents the groundwater component. Eventually, a triangular routing function is applied to the runoff components to determine the final discharge. The TUWmodel has 15 parameters that need to be calibrated against streamflow data (See Table S1 in the Supplement for prior parameter ranges).

2.4.2 GR4J

The GR4J model (https://cran.r-project.org/web/packages/airGR/, last access: 10 February 2022, Perrin et al., 2003) was used in our study with the additional snow module of Valéry et al. (2014). At first, the snow module determines the amount of melt water and liquid rainfall. If the rainfall and snowmelt exceed the potential evaporation, the net precipitation is determined by subtracting the potential evaporation from the rainfall and snowmelt, and the net available potential evaporation is set to zero. Conversely, if the rainfall and snowmelt are less than the potential evaporation, the net precipitation is set to zero and the net available potential evaporation is determined by subtracting the rainfall and snowmelt from the potential evaporation. Afterwards, a part of the net precipitation enters a reservoir, defined as the production store, based on the current level of storage in this reservoir.

Also, this model does not consider vegetation explicitly. Here, vegetation is related to the top reservoir, the production store, with the transpiration as function of the actual levels in this reservoir:

$$E_t = \frac{S\left(2 - \frac{S}{x_1}\right) \tanh\left(\frac{E_n}{x_1}\right)}{1 + \left(1 - \frac{S}{x_1}\right) \tanh\left(\frac{E_n}{x_1}\right)}, \qquad (9)$$

with S the actual storage (mm), E_n the net available potential evaporation (as described above) (mm d^{-1}), and x_1 a constant calibration parameter defining the maximum storage capacity (mm).

From the production store, water can also percolate down. Eventually, the percolated water is added to the part of the precipitation that did not enter the production store, and this sum of water is divided into two flow components. Of it, 90 % is routed by a unit hydrograph and a non-linear routing store, whereas 10 % is routed by a single unit hydrograph. The two routed components are summed again to obtain the resulting discharge. The GR4J model with the additional snow module has in total six model parameters for calibration.

2.4.3 FLEX

The last hydrological model (https://github.com/rcnijzink/flexsimple/, last access: 10 February 2022, Nijzink, 2022) used in this study is based on the FLEX model as originally described by Fenicia et al. (2006). At first, a snow module is run to determine the amount of water that enters the interception reservoir. From there, the water either evaporates directly, or, when a storage threshold is exceeded, the water continues to the unsaturated reservoir or to the overland flow reservoir. This model does not specifically model vegetation either, but the water fluxes related to vegetation result mainly from the unsaturated storage. Depending on the current state in the unsaturated storage, water can infiltrate into the unsaturated reservoir or is added to a fast flow reservoir. Evaporation takes place from the unsaturated reservoir as well, based on the amount of water stored here:

$$E_T = \begin{cases} \frac{S_u}{LP \cdot S_{u,\max}} \cdot E_p, & \text{if } S_u < \text{LP} \cdot S_{u,\max} \\ E_p, & \text{if } S_u < \text{LP} \cdot S_{u,\max}, \end{cases} \qquad (10)$$

with S_u the soil moisture state (mm), $S_{u,\max}$ a constant calibration parameter reflecting the maximum soil moisture storage (mm), and LP a constant calibration parameter reflecting the relative soil moisture threshold after which evaporation occurs at a potential rate (–). Besides evaporation, percolation occurs as well from the unsaturated reservoir, based again on the amount of water in the unsaturated zone. The percolated water adds to the last reservoir, which mimics the slow component of the groundwater. The FLEX model has 14 free parameters for calibration.

2.4.4 Calibration strategy for the conceptual hydrological models

The three hydrological models were each run with 50 000 random parameterizations for the six Australian catchments. This was done in order to find the most suitable parameter set, which is defined here as the parameter realization that achieves the highest Kling–Gupta efficiency (KGE, Gupta et al., 2009) for reproducing observed discharge during the calibration period. The full time series are used for the calibration period after omitting the first warm-up year. The

Table 3. Calibrated parameters related to vegetation (note: not all the calibrated parameters) in the FLEX, TUW, and GR4J model. See Supplement S6 for all calibrated model parameters.

FLEX			
Parameter	Description	Initial range	Unit
I_{max}	maximum interception capacity	0.0–50.0	mm
$S_{u,max}$	maximum root zone storage capacity	1.0–1000.0	mm
beta	shape factor soil moisture function	0.01–20	–
Kf	recession coefficient fast reservoir	1.0–30.0	days
Ks	recession coefficient slow reservoir	30.0–1000.0	days
LP	filling of soil moisture after which transpiration equals the potential rate	0.00–1.0	–
TUW			
LPrat	parameter related to the limit for potential evaporation	0.00–1.0	–
FC	field capacity, max. soil moisture storage	0.0–600.0	mm
BETA	non-linear parameter for runoff production	0.00–20.0	–
GR4J			
x_1	maximum capacity of the production store	20–300	mm

models were run for the full length of the time series as specified in Table 2.

2.5 Experimental design

The general approach was to first run the models using site-specific meteorology, and then conduct several numerical experiments where only precipitation is increased or decreased by a constant factor, while all other meteorological variables and model parameters remain unaltered. Precipitation was chosen as a representation of climate change, as it affects all models in a similar way, whereas potential evaporation is not used as input for the VOM. Since the VOM requires extended meteorological input over the entire modeling period (solar irradiance, vapor pressure), whereas the conceptual hydrological models require streamflow data for calibration, they were run for different sets of sites, with only the six catchments in Australia providing adequate input data for all models. For the Australian catchments and flux tower sites, the positions in the Budyko framework for the VOM and the hydrological models were all determined for the period 1 January 1985 until 31 December 2005 for consistency.

The steps of the experiment are summarized in Fig. 2. First, the base steps of the experiment were as follows.

- *Optimization VOM.* The VOM was fully optimized for the flux tower sites, the 36 additional locations along the NATT, and the six Australian catchments for the meteorological data as observed.

- *Calibration of hydrological models.* The three hydrological models, FLEX, TUWmodel, and GR4J, were calibrated (see Sect. 2.4.4) for the six catchments in Australia, using the observed site-specific meteorological data as input, and correspondence with observed streamflow as the calibration target in terms of the highest Kling–Gupta efficiency (KGE, Gupta et al., 2009), see also Sect. 2.4.4. Supplement S3 contains an additional analysis where this was repeated for 357 catchments in the US to assess the behavior of the hydrological models also for a larger set of catchments with different climates and vegetation.

In the next step, the meteorological forcing was altered by multiplying the precipitation (P) with factors ranging from 0.2 to 2.0 in steps of 0.2. The models were run with the optimized vegetation properties (VOM) or calibrated model parameters (hydrological models) from the first step, specifically as follows.

- *Re-run the VOM for each P scenario.* The VOM was run for each P scenario with the vegetation parameters that were obtained in the unmodified situation based on observed P, representing perturbations in climate where long-term vegetation properties are not (yet) affected by changes in P.

- *Run the VOM for each P scenario without vegetation.* The VOM was also run without vegetation (i.e., only soil evaporation) for the different P amounts.

- *Re-run the hydrological models for each P scenario.* Similarly, the conceptual hydrological models were run for each P scenario as well, using the parameters that were calibrated to the unmodified situation.

In the third and last step, it was assumed that vegetation has fully adapted to each perturbation of precipitation. This was only possible for the VOM.
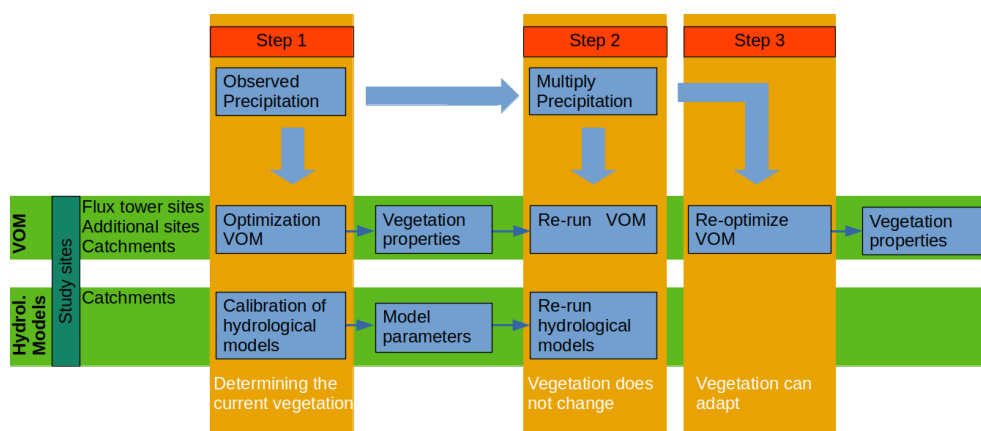
Figure 2. Flow chart of the experimental design, see description Sect. 2.5.

– *Re-optimize the VOM for all P scenarios.* The VOM was re-optimized for all P scenarios at each of the Australian study sites (i.e., catchments, flux tower sites, and additional locations), representing perturbations in rainfall where vegetation has fully adapted to each perturbation.

The hydrological models were not run in this last step, as there is no way to represent the adaptation of vegetation to a hypothetical situation in these models.

3 Results

3.1 VOM simulations with unperturbed rainfall

VOM simulations with optimized vegetation properties led to a closer convergence along the Budyko curve and higher n values than VOM simulations without vegetation (Fig. 3). For the flux tower sites where observations of λE were available (Fig. 3a), the optimized VOM plotted much closer to the flux tower observations than the VOM runs without vegetation. At the same time, the curve fit for Eq. (3) was much better for the optimized VOM, as indicated by the lower mean square error (3.86×10^{-3} vs. 2.004×10^{-2}). The 36 additional locations along the NATT (Fig. 3b) and the six Australian catchments (Fig. 3c) also resulted in higher n values for the optimized vegetation compared to no vegetation, as well as a higher convergence to the curve (lower mean squared errors, with 1.788×10^{-3} vs. 2.339×10^{-2} and 1.249×10^{-3} vs. 5.504×10^{-3}, for the curves with and without optimized vegetation, respectively).

3.2 Optimal vegetation response to modified precipitation

Simulated responses to systematic shifts in precipitation (P) only tracked along the Budyko curve at individual flux tower sites if vegetation was re-optimized (i.e., green and gray sym-

bols did not plot along the lines of the same color in Fig. 4, but the black symbols plotted much closer to their curve). This is also evident in the substantially lower mean squared errors for the black lines (see figure legends). The deviations from the Budyko curves were systematic, in that simulations with reduced P (higher $Rn/\lambda P$) fell above the curve and simulations with higher P (lower $Rn/\lambda P$) fell below the curve.

The n value fitted for 36 additional locations along the NATT similarly reduced from 1.183 to 1.095 after increasing the total rainfall by 20 % if the long-term vegetation properties were not re-optimized (Fig. 5). After re-optimizing the vegetation properties in the VOM for the increased precipitation, n returned close to its original value for unperturbed precipitation (black triangles in Fig. 5, with an n value of 1.176). This was associated with increased values of the water-use parameters ($c_{\lambda f,\mathrm{p}}$ and $c_{\lambda e,\mathrm{p}}$), vegetation cover, and rooting depth of the perennial vegetation (Fig. 6a), whereas the seasonal vegetation parameters changed less. Re-optimization for increased P also resulted in greater water and carbon fluxes in the VOM, which was more pronounced for the perennial than the seasonal vegetation (Fig. 6b).

The simulated responses to changes in precipitation (P) at six Australian catchments revealed that the re-optimized VOM followed a Budyko curve most closely (i.e.,lowest values of the mean square error, Fig. 7) compared with the conceptual hydrological models FLEX, TUWmodel, and GR4J (see Supplement S3, Fig. S3.1–S3.7 for time series of meteorological data, model performances, and resulting discharges). The hydrological models, with the same model parameters for each P scenario, deviate from the Budyko curve in a similar way as the VOM without re-optimization (too flat around the unperturbed P). When the hydrological models were run for a selection of CAMELS catchments (see Supplement S3, Fig. S3.8–S3.11), their n values also reduced for
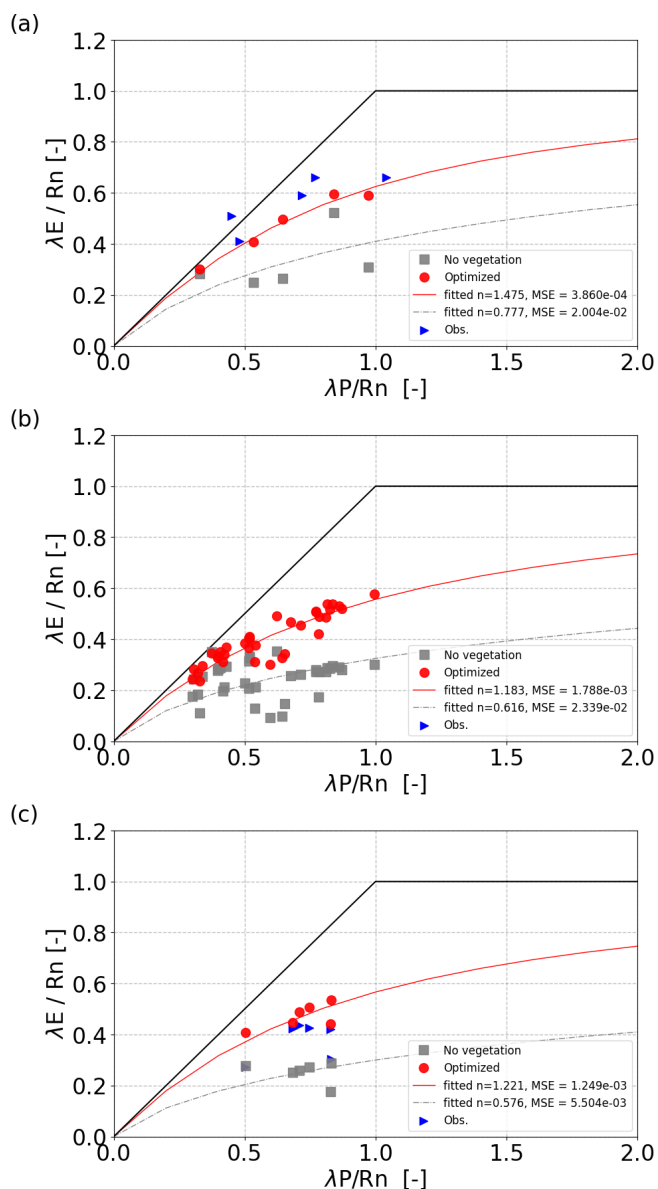
Figure 3. Results of the VOM in Budyko space for **(a)** flux tower sites along the North Australian Tropical Transect (NATT), **(b)** 36 additional points around the NATT, and **(c)** six catchments around the NATT. The VOM with fully optimized vegetation is shown in red dots, the VOM run without vegetation (bare soil) in gray squares, and observations (from flux tower data **a** or runoff data **c**) in blue triangles. Lines are fits of Eq. (3) to the data points of the same color.

a 20 % increase in precipitation and constant model parameters, but these changes remained relatively small.

3.3 Sensitivity of site-specific n values to changing precipitation

In the next step, the n values were treated as site-specific properties, and the sites and catchments were each fitted to

Eq. (3) individually and per precipitation (P) scenario (i.e., a separate n value for each data point in Figs. 4 and 7). The n values resulting from re-optimized long-term vegetation properties for each P scenario were considerably less variable at each site than those obtained for constant long-term vegetation properties, both at each NATT site (Fig. 8) and across the 36 additional sites along the NATT (Fig. 10a). For these sites, increasing precipitation by 20 % without re-optimizing the vegetation resulted in a reduction in n values by around 0.10 (blue box, Fig. 10a), whereas the re-optimized VOM simulations (red box, Fig. 10a) did not result in a systematic change in n. Surprisingly, for re-optimized vegetation, the variation in n between sites was greater than at each individual site, even though P was varied by an order of magnitude (Figs. 8 and 9a). The opposite was the case if the long-term vegetation properties were not re-optimized for each perturbed P (Figs. 8 and 9b), or if the conceptual hydrological models with constant parameters were used (Fig. 9c–e). In all these latter model simulations, the n values systematically declined with positive perturbations in P and increased with negative P perturbations. In an additional analysis, the three hydrological models were applied to a selection of catchments of the CAMELS data to prove the generality of our findings. Interestingly, in this analysis we found that the sensitivity of n to changes in P was relatively similar (median decrease in n by 0.1 in response to a 20 % increase in P) compared with the non-optimized VOM (Fig. 10a), although the models were run over very different sets of conditions, i.e., the CAMELS catchments in the US for the hydrological models and sites along the NATT in Australia for the VOM (see also Supplement S3, Fig. S3.8–S3.11 for all results).

4 Discussion

The results of our study provided new insights into the likely principles underlying convergence of catchments along the Budyko curve and shed new light into the expected sensitivity of vegetation and the catchment water balance to changes in climate. Here we systematically discuss the questions raised and hypotheses formulated in the introduction, before proceeding to more general observations and limitations of this and similar studies.

4.1 Reproduction of the Budyko curve by optimality

The first hypothesis formulated in the introduction (H1) is that convergence of catchments along the Budyko curve, i.e., close to the maximum possible long-term evapotranspiration, results from vegetation optimality.

H1: model simulations based on vegetation optimality lead to a better reproduction of the empirical Budyko curve than model simulations without self-optimized vegetation.
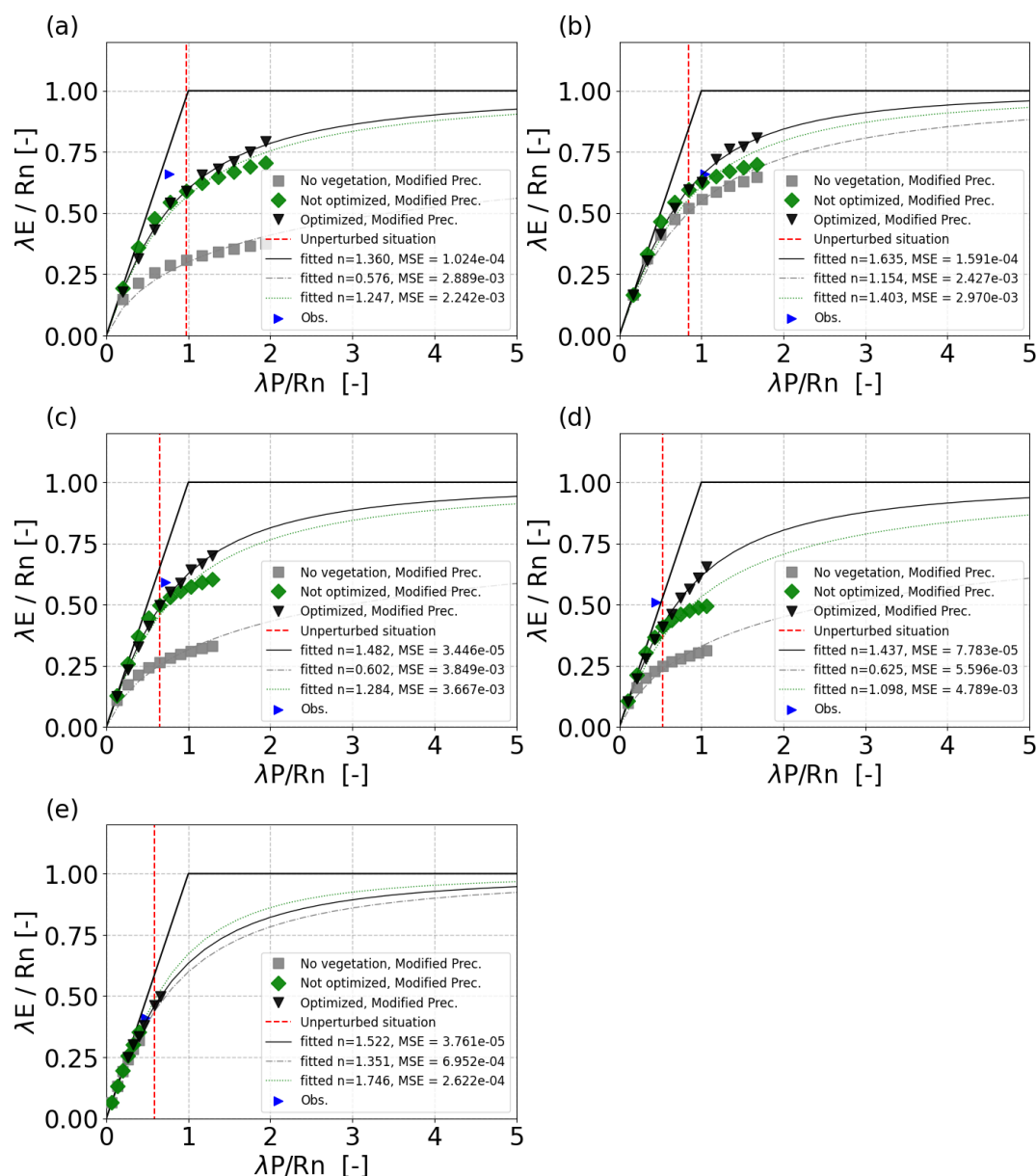
Figure 4. VOM results along the NATT in Budyko space as a result of modified precipitation for **(a)** Howard Springs, **(b)** Adelaide River, **(c)** Daly Uncleared, **(d)** Dry River, and **(e)** Sturt Plains. Gray squares denote simulations without vegetation (bare soil), black triangles denote fully optimized simulations, and green diamonds denote simulations where the VOM was run with the optimal vegetation properties determined for an unmodified climate. The unmodified climate is indicated by the dashed red line. The blue triangles denote the eddy covariance observations summed over the available period for each site. Lines are fits of Eq. (3) to the data points of the same color.

This hypothesis is clearly supported by the following findings: (a) the VOM with fully optimized vegetation follows more closely Budyko curves with realistic n values (1.1–1.5) than the VOM without vegetation (Fig. 3). In comparison, literature n values often range between 1.5 and 2.6 (e.g., Roderick and Farquhar, 2011; Choudhury, 1999; Yang et al., 2008). Note that the values found here are lower than the recommended value of 1.8 by Choudhury (1999) or the value of 2.0 used in the Turc–Pike relationship (Pike, 1964), but

compare well with the n value of 1.49 found by Williams et al. (2012) for 176 flux tower sites. In contrast, the n values of 0.62–0.78 produced by the VOM simulations without vegetation (bare soil evaporation only) are well below any values reported in the literature. Many other authors have shown previously that the evaporative fraction decreases due to land clearing. In fact, Li et al. (2013) found a positive relation between the curve shape parameter and vegetation cover, implying an increasing evaporative fraction with in-
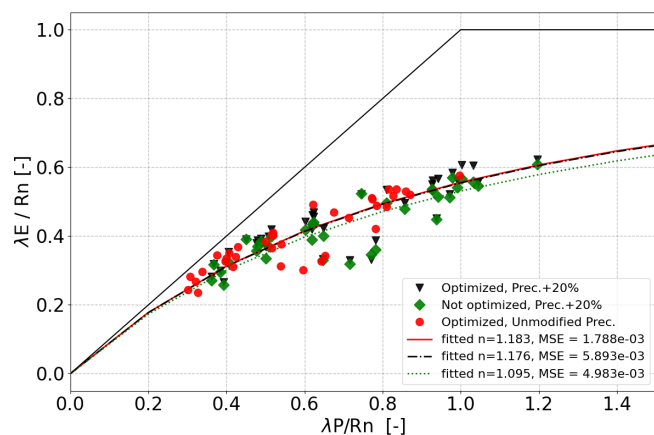
Figure 5. VOM results along the NATT in Budyko space as a result of modified precipitation for 36 additional locations. Black triangles denote fully optimized simulations with modified precipitation, while green diamonds denote simulations where the VOM was run with the optimal vegetation properties determined for an unmodified climate (red dots). Lines are fits of Eq. (3) to the data points of the same color.

creasing vegetation cover. As discussed below, our results suggest on top of this that for a changing climate, this shape parameter would only be conserved if vegetation is free to co-evolve with the climate, which would not be the case in a cleared catchment. (b) Simulations with perturbed precipitation (P) revealed that the VOM with re-optimized vegetation for each P setting followed the same Budyko curve very closely, whereas none of the other models did (Figs. 4, 5 and 7). This happened consistently for different study sites and will be discussed in more detail in the next section.

Altogether, these results suggest that vegetation optimality has a strong tendency to push the catchment water balance closer towards the envelope compared to simulations without vegetation, but also to keep it on a catchment-specific Budyko curve as climate changes (n varied more between catchments than within each catchment as P was varied by an order of magnitude in Fig. 8). So far, the Budyko framework was related to optimality theory only a few times, mostly by applying thermodynamic optimality principles and constraints in numerical experiments (Porada et al., 2011; Kleidon et al., 2014; Westhoff et al., 2016; Wang et al., 2015). To our knowledge, the results presented here illustrate for the first time that an ecologically motivated optimality principle (maximum net carbon profit) leads to a close reproduction of the Budyko curve. Previously, Milly (1994) suggested that convergence towards the Budyko curve may be a result of plants optimizing their rooting depths to maximize transpiration in a given environment. However, here we found that convergence on the Budyko curve is likely the result of rooting depths, vegetation cover, and water-use strategies playing together in a way to satisfy a biological optimality principle.

4.2 Sensitivity of *n* values to changes in precipitation

Our second hypothesis (H2) reflects a common belief expressed in the literature whenever the Budyko framework is used to study the effects of climate change.

H2: the empirical parameter n stays constant as climate changes, as long as vegetation cover and rooting depths stay constant.

Based on our results for varying precipitation (P), this hypothesis has to be clearly rejected. Constant long-term vegetation properties in the VOM and constant parameters in the conceptual hydrological models led to a large spread in n values, with a systematic decline in n for increasing P and increase in n for reduced P (Figs. 8, 9). In our study, only full optimization of vegetation properties to changing precipitation led to a constant n as P was changed step-wise, by up to an order of magnitude (Figs. 8 and 9a). But this optimization, in fact, represents a change in vegetation properties as P changes, disproving the above hypothesis in the context of the four models applied in the present study. Interestingly, the VOM with constant vegetation properties and the conceptual models showed similar responses to perturbations of precipitation, even though these models are extremely different in nature. The VOM specifically models photosynthesis by representing the vegetation as two big leaves, resulting in carbon and water exchange with the atmosphere, whereas the conceptual hydrological models simulate vegetation in a more simple manner. In these models, the root zone storage capacity is often seen as the key variable determining the vegetation-related fluxes (e.g., Gao et al., 2014; Wang-Erlandsson et al., 2016). Note that the rooting depths of the VOM along with the soil water retention curves could be used to calculate root zone storage capacities, which would have a similar meaning to those in the conceptual models, but such a comparison and its interpretation is beyond the scope of this study. The conceptual hydrological models do not differ strongly between each other in their formulations of transpiration, but they do differ in their representations of hydrological processes, such as overland flow and interception evaporation (included in the FLEX model), or their number of free calibration parameters (e.g., just six for the GR4J model).

However, our findings bring forward one of the main deficiencies that many conceptual hydrological models currently have, namely the missing ability to adjust system properties (i.e., parameters) in response to environmental change, an ability that would be needed for predictions under change (Montanari et al., 2013; Ehret et al., 2014). Calibrating conceptual model parameters to past observations and then using the calibrated models for prediction under environmental change implicitly assumes that the model parameters represent static catchment properties, which should not change as, e.g., the climate changes. The flaw in this assumption becomes immediately clear if one considers that some of these parameters encode vegetation functioning, which cannot be
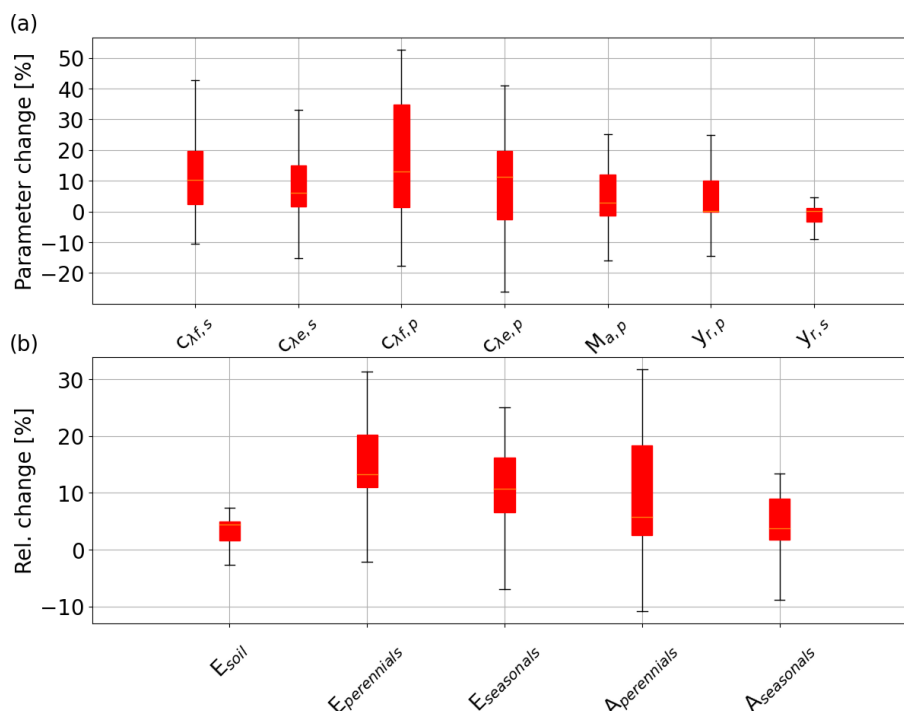
Figure 6. Simulated changes in response to a 20 % increase in precipitation in the VOM (based on Fig. 4) for **(a)** optimized vegetation properties, with the water-use parameters for perennial ($c_{\lambda f,p}$ and $c_{\lambda e,p}$) and seasonal vegetation ($c_{\lambda f,s}$ and $c_{\lambda e,s}$), perennial vegetation cover ($M_{A,p}$), and root depths for the perennial and seasonal vegetation ($y_{r,p}$ and $y_{r,s}$); and **(b)** fluxes with soil evaporation (E_{soil}), transpiration of perennial trees ($E_{perennials}$), transpiration of seasonal grasses ($E_{seasonals}$), gross primary productivity (GPP) of perennial trees ($A_{perennials}$), and GPP of seasonal grasses ($A_{seasonals}$).

assumed static as the environment changes. The VOM and other process-based models offer a clearer separation between parameters related to physical catchment properties and those encoding vegetation functioning. Especially the optimality part enabled the VOM to track the Budyko curve under changing P, which is very encouraging for the implementation of vegetation optimality for predictions under change, as already shown for predicting vegetation response to elevated CO_2 (Schymanski et al., 2015).

4.3 Long-term vegetation response and resulting n values

The last hypothesis relates to the underlying reasons for a change in n values.

H3: changes in n values are a result of slowly varying, long-term vegetation properties.

As already hinted at in the previous section, this hypothesis has to be rejected too as our results suggest the opposite. Only if the slowly varying, long-term vegetation properties were re-optimized in response to changing precipitation (P) did n stay constant, otherwise n changed in the opposite direction to P (Fig. 6). This seems in line with the long-term character of the Budyko curve itself, but actually conflicts with findings that variations around the curve correlate with

variations of the long-term average annual vegetation coverage (Li et al., 2013), forest cover (Shao et al., 2012), or fPAR values (Zhang et al., 2016). Interestingly, the simulated changes in rooting depths in response to increased P (Fig. 6) agree with the general observation that rooting depths increase with increasing precipitation amounts (Schenk and Jackson, 2002). In a previous study, we found that the VOM reproduces this pattern along a precipitation gradient (Nijzink et al., 2022a), whereas here we demonstrate that the VOM also maintains this pattern over time for constant physical catchment properties.

Our finding that n varied less in response to changes in P than between catchments (Fig. 8) suggests that the n values are indeed site-specific. However, our analysis did not reveal whether n depends on properties of climate (e.g., temperature, seasonality of net radiation and precipitation, rainfall intensity), physical catchment properties (e.g., soil water-holding capacity), or both. Previous studies also suggested that n is a catchment-specific variable depending on climate properties (other than mean annual P and R_n), physical catchment properties, and/or vegetation (Donohue et al., 2007; Oudin et al., 2008; Yang et al., 2009; Williams et al., 2012).

However, our findings challenge the common belief formulated in H3 that changes in n are a result of changes in
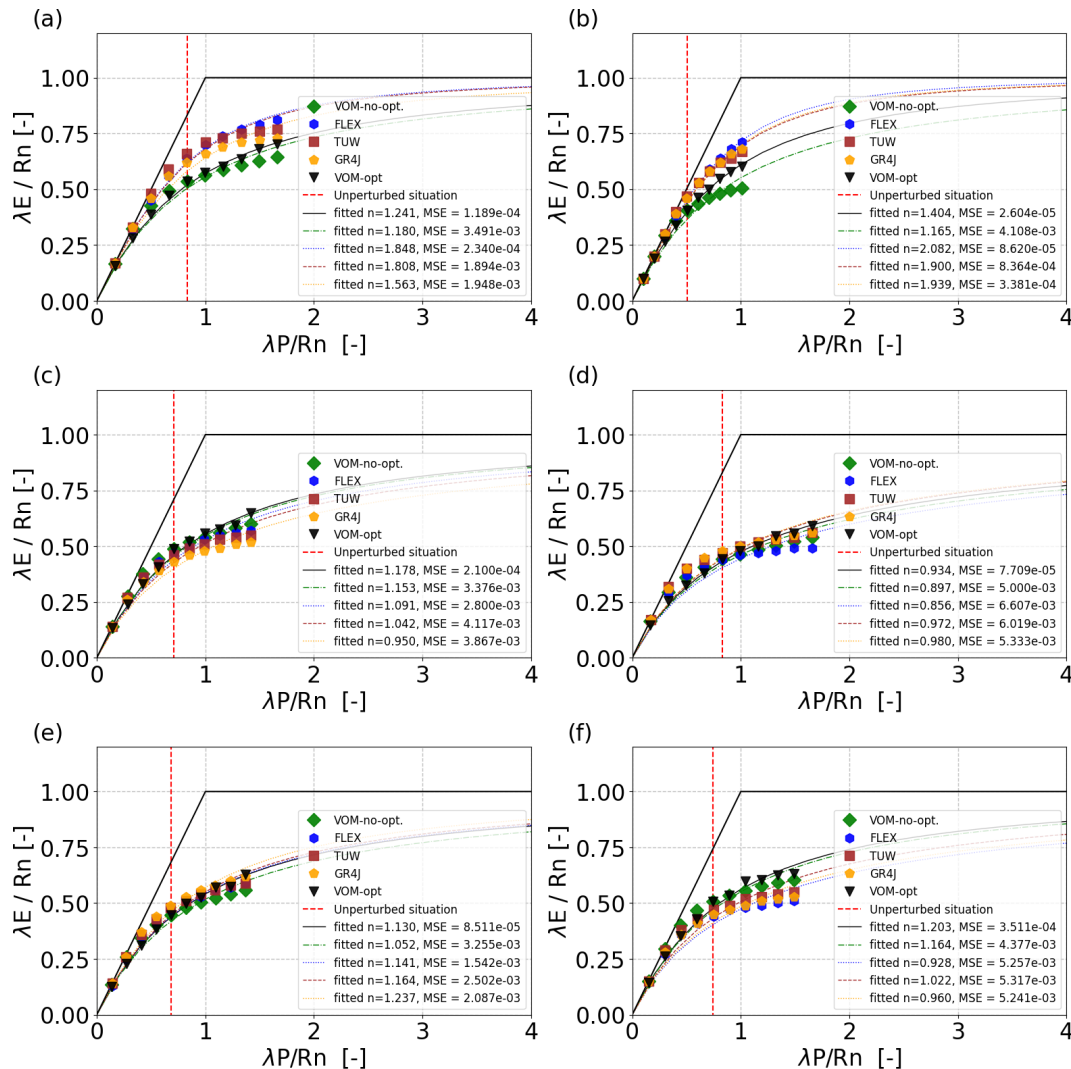
Figure 7. Simulations in Budyko space for six catchments in Australia as a result of modified precipitation for the optimized VOM (black stars), VOM without optimization (green triangles), FLEX (red diamonds), TUWmodel (gray dots), and GR4J (gold squares) for **(a)** Adelaide River, **(b)** Dry River, **(c)** Fergusson River, **(d)** Magela Creek, **(e)** Seventeen Mile Creek, and **(f)** South Alligator River. The unmodified climate is indicated by the dashed red line.

the physical catchment properties or vegetation, whereas n should stay constant if only mean annual P or R_n change (Roderick and Farquhar, 2011; Renner et al., 2012). Our results suggest quite the opposite, as changes in the long-term, slowly varying vegetation properties were needed to bring a certain catchment back to the original n value after a change in P. Since vegetation reacts to the climate, the parameter n can be considered a combined result of climate, vegetation, and landscape properties (Zhang et al., 2004; Roderick and Farquhar, 2011; Donohue et al., 2012; Ning et al., 2017). In some studies, n values were found to correlate stronger with catchment properties (e.g., Yang et al., 2014), but one could argue that catchment properties influence vegetation and vice versa. Interestingly, vegetation optimality suggests that the vegetation response to changes in climate stabilizes

n. Our results also emphasize that the dynamic evolution of the system is important, as argued before by, e.g., Koster and Suarez (1999) and Yang et al. (2007). If a climatic shift happens quickly, and the state of the system did not yet adapt to the new situation, we may expect different n values than for a system in a (dynamic) steady-state. Note that other authors were not able to find that catchments followed a single Budyko trajectory over time (Reaver et al., 2022).

4.4 Dryness and wetness index

Different ways to plot the Budyko framework have been used in the literature, either using a dryness index ($R_n/\lambda P$) or a wetness index ($\lambda P/R_n$) as the independent variable. For this reason, we repeated our analyses in Supplement S4 for dif-
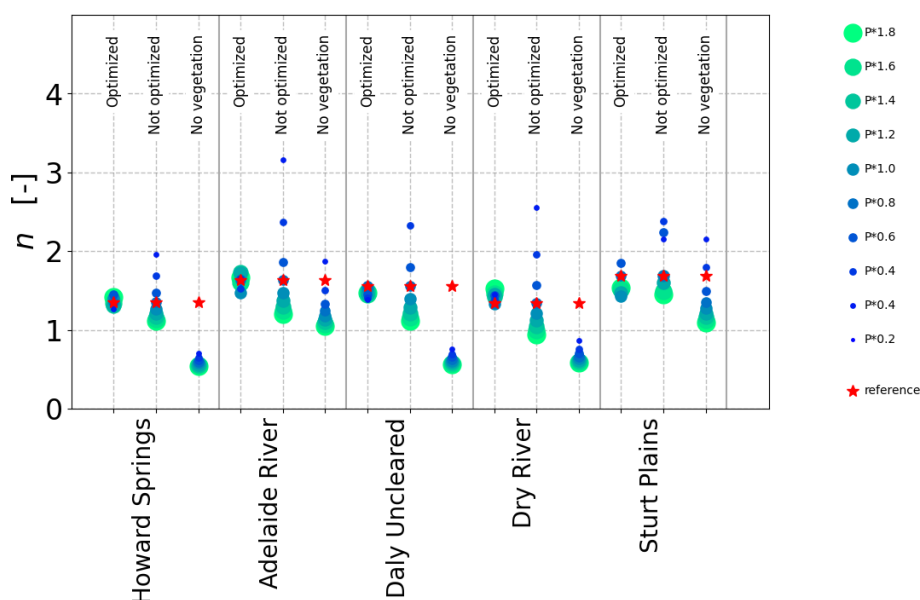
Figure 8. Variability of n in response to changing precipitation in the VOM. A separate n value was fitted to each point in Fig. 4. Sizes of dots represent the multiplication factor by which precipitation was modified at each site, while the red stars indicate simulations with unmodified precipitation. "Optimized": fully optimized vegetation, "not optimized": optimal vegetation properties of unmodified precipitation, and "no vegetation": bare soil simulations.

ferent projections of the Budyko framework. The previous results in Sect. 3.1–3.2 remained valid after using a Budyko space based on a dryness index (Fig. S4.1–S4.5 in Supplement S4). Nevertheless, it must be noted that the resulting n values differ for a Budyko space with a wetness index instead of a dryness index. More specifically, Fig. S4.5 shows, for example, that the resulting n values for the CAMELS data slightly differ. However, the n values still similarly change for a Budyko plot with the dryness index $\lambda P/R_n$ as the independent variable as for a Budyko plot with a wetness index (Supplement S3, Fig. S3.8).

Note also that the results in Sect. 3.3 would not change for a different Budyko projection, as these n values could be solved analytically. However, when using a dryness index (i.e., plotting E/P as a function of $R_n/\lambda P$), the interpretation of the results becomes more difficult, as e.g., an increased P would decrease E/P at constant E. Therefore, changes in E do not directly translate to changes in E/P. For this reason, we used a wetness index in the main paper (i.e., plotting $\lambda E/R_n$ as a function of $\lambda P/R_n$), in which case a change in P only results in a change on the vertical axis if E changes.

4.5 Limitations

In the present study, we perturbed precipitation in isolation, i.e., without perturbing any other climate variables, which does not reflect any realistic climate change scenario. Moreover, changes in precipitation are in reality linked to changes in vapor pressure, net radiation (e.g., through cloud forma-

tion), air temperatures, stronger sensible heat fluxes, warmer and drier soils, and likely also different rainfall intensities. We also attempted to vary atmospheric water demand but were limited by the differences of the VOM and conceptual hydrological models. The hydrological models use potential evaporation as input, whereas the VOM uses vapor pressure, temperature, and incoming shortwave radiation to drive evaporation. VOM simulations with altered vapor pressure and incoming shortwave radiation are presented in Supplement S2. Especially when altering the vapor pressure, results became difficult to interpret, as net longwave radiation and hence the position along the x axis of the Budyko plots is only indirectly affected by vapor pressure (Eq. 39, Allen et al., 1998). Here, the results strongly depended on the projection in Budyko space, i.e., whether a dryness or wetness index was used (see Supplement S2, Fig. S2.3). In contrast, changes in shortwave radiation confirmed that vegetation optimality reduces departures from the Budyko curve compared to static vegetation (Supplement S2, Fig. S2.1 and S2.2), but in a less systematic way than precipitation. This related to shortwave radiation being a strong driver for photosynthesis in the VOM, which profoundly affects all components of vegetation.

As the study used 37 years of data, changes at the study sites during this time window may have occurred. The flux tower sites are relatively undisturbed, but suffer occasionally from fires (Beringer et al., 2007; Hutley et al., 2011). At the same time, at Howard Springs it has been noted that trends exist in gross primary productivity and water-use efficiency (Hutley et al., 2022). Also at the catchments and additional
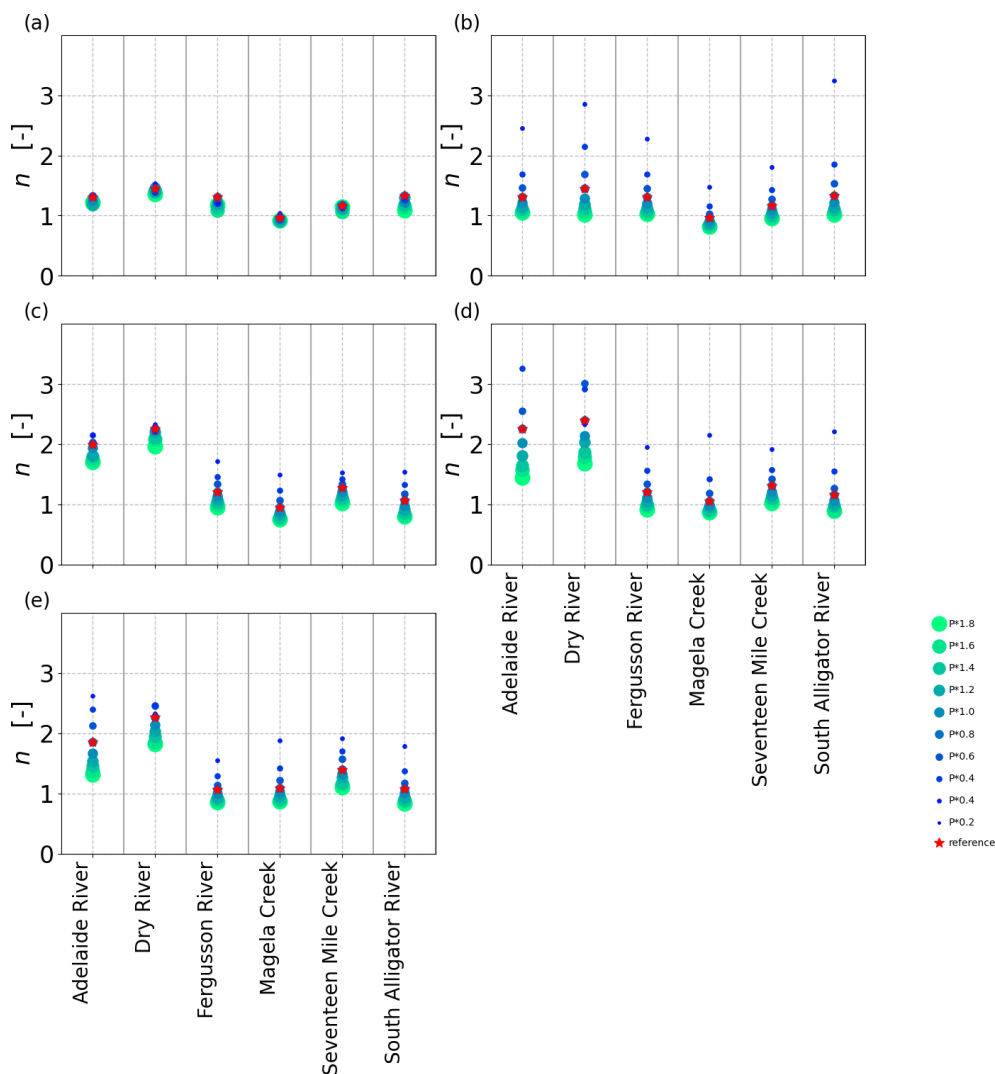
Figure 9. Variability of n in response to changing precipitation in **(a)** the optimized VOM, **(b)** the VOM without re-optimization, **(c)** FLEX, **(d)** TUWmodel, and **(e)** GR4J. Fitted n values for six catchments in Australia with unperturbed precipitation (red star) and increased/decreased precipitation (color scale).

locations along the transect, changes and trends may have occurred during this period. However, only the full time series of the climate data were used as input for the numerical experiments, and hence any trends would not make a difference to our final results. Note also that discrepancies between flux tower observations (i.e., blue triangles in Fig. 3) and model results relate to the long-term character of the Budyko framework, with flux tower time series being much shorter than the simulated time series.

The VOM and the hydrological models used in this study are spatially lumped so they should not be expected to adequately represent the water and energy partitioning of large heterogeneous catchments. Here we just used these models as simplified representations of the key processes determining this partitioning and to test our general hypotheses about the Budyko curve.

The range of hydrological models used in this study is extremely limited. Many hydrological models use more complex approaches to model evapotranspiration, which are likely better suited for climate change studies. Here, three relatively simple models were chosen to test the robustness of our finding that changing precipitation leads to changing n if vegetation does not adapt. The changing n in these simple models without explicit vegetation component illustrates most convincingly that the change is not brought about by vegetation processes, as suggested in the literature previously.

This study did not aim to predict responses of vegetation and the water balance to any realistic climate change scenario, and the finding of a stabilizing effect of vegetation optimality on the value of n as precipitation changes may not apply to human-induced climate change at all. This is
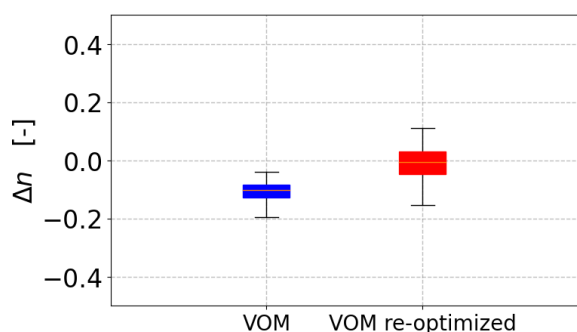
Figure 10. Changes in n in response to a 20 % increase in precipitation (P). VOM simulations are shown in for 36 sites along the NATT, with the blue box (left) representing VOM simulations where the long-term vegetation properties were not re-optimized to the increased P and the red box (right) representing simulations where all vegetation properties were re-optimized for the increased P. The n values were obtained by fitting Eq. (3) to each individual site for a given P scenario.

most obvious when considering that rising atmospheric CO_2 concentrations are the main driver of human-induced climate change, as they have a profound, direct effect on vegetation water use (which can be buffered, enhanced, or even reversed by vegetation optimality, depending on the climate), which would modify a site-specific n value permanently, even in the absence of any other climatic changes (Schymanski et al., 2015).

5 Conclusions

The Vegetation Optimality Model showed a strong convergence to the empirical Budyko curve for six eddy covariance sites, 36 additional locations along the North Australian Tropical Transect, and six catchments in Australia, if vegetation was re-optimized for perturbations in precipitation. In contrast, the VOM with constant vegetation properties, as well as three hydrological models with constant parameters, led to systematic changes of the parameter n defining the curve, with increased n values for decreased precipitation and decreased n values for increased precipitation.

Our study results have a range of potentially important implications. First of all, the finding that vegetation optimality explains convergence of catchments on the empirical Budyko curve lends support to further explore optimality principles for the prediction of vegetation water use in ungauged situations and in a changing environment. Secondly, if the vegetation response to changes in precipitation (P) indeed follows the predictions of the VOM, we may use the Budyko framework for predicting sensitivities of the catchment water balance to P as was done in several previous studies. However, our results motivate an expectation that n should be conserved at a given catchment in the long term, whereas it may vary in the short to medium term as climate changes.

This highly contrasts with previous assumptions that the parameter n should stay constant in the short term as climate changes, and then vary in the longer term. Nevertheless, the long-term conservation of n would make the Budyko framework even more useful, as long-term predictions are notoriously difficult.

Furthermore, we found that vegetation adaptation to climatic change may not always lead to an increase in transpiration, but also to down-regulation of vegetation properties, depending on the type and direction of climate change. For example, in our study, the VOM and all other models predicted that increases in P would reduce n while decreases in P would increase n, if vegetation does not fully adapt to the new P. This means that in a climate change scenario with reduced P, vegetation water use may keep decreasing slowly as vegetation re-adjusts its rooting depth, cover, and water use strategies to the new setting, bringing n back to its original value.

However, climate change never affects only one aspect of atmospheric forcing and given that, e.g., rainfall intensity and seasonality of water and energy availability has an impact on n, the assumption of constant n as climate changes may not be adequate. Moreover, one important aspect of climate change has not been touched upon at all in this study, which is the effect of rising atmospheric CO_2 concentrations, which may have a lasting effect on n all by themselves, on top of their effect on local climate. For that reason, we advocate the inclusion of CO_2 concentrations in any analysis of climate change effects on vegetation water use. Nevertheless, our finding that vegetation optimality tends to keep n close to a site-specific value serves as a strong motivation to investigate further what aspects of climate and physical catchment properties most likely affect this value, as such knowledge may enable robust predictions about changes to the water balance in response to climate change.

References

Addor, N., Newman, A. J., Mizukami, N., and Clark, M. P.: The CAMELS data set: catchment attributes and meteorology for large-sample studies, Hydrol. Earth Syst. Sci., 21, 5293–5313, https://doi.org/10.5194/hess-21-5293-2017, 2017.

Allen, R. G., Pereira, L. S., Raes, D., and Smith, M.: Crop evapotranspiration – Guidelines for computing crop water requirements, Irrigation and drainage paper 56, FAO – Food and Agriculture Organization of the United Nations, Rome, ISBN 92-5-104219-5, 1998.

Bergström, S.: Development and Application of a Conceptual Runoff Model for Scandinavian Catchments, Tech. rep., SMHI, SMHI Rep. RHO 7, https://www.smhi.se/polopoly_fs/1.163091!/RHO_7 Development and application of a conceptual runoff model for Scandinavian catchments.pdf (last access: 1 December 2022), 1976.

Beringer, J., Hutley, L. B., Tapper, N. J., and Cernusak, L. A.: Savanna fires and their impact on net ecosystem productivity in North Australia, Glob. Change Biol., 13, 990–1004, https://doi.org/10.1111/j.1365-2486.2007.01334.x, 2007.

Budyko, M.: Climate and Life, Academic Press, New York and London, edited by: Miller, D. H., ISBN 9780121394509, 1974.

Choudhury, B.: Evaluation of an empirical equation for annual evaporation using field observations and results from a biophysical model, J. Hydrol., 216, 99–110, https://doi.org/10.1016/S0022-1694(98)00293-5, 1999.

Donohue, R. J., Roderick, M. L., and McVicar, T. R.: On the importance of including vegetation dynamics in Budyko's hydrological model, Hydrol. Earth Syst. Sci., 11, 983–995, https://doi.org/10.5194/hess-11-983-2007, 2007.

Donohue, R. J., Roderick, M. L., and McVicar, T. R.: Deriving consistent long-term vegetation information from AVHRR reflectance data using a cover-triangle-based framework, Remote Sens. Environ., 112, 2938–2949, https://doi.org/10.1016/j.rse.2008.02.008, 2008.

Donohue, R. J., Roderick, M. L., and McVicar, T. R.: Roots, storms and soil pores: Incorporating key ecohydrological processes into Budyko's hydrological model, J. Hydrol., 436–437, 35–50, https://doi.org/10.1016/j.jhydrol.2012.02.033, 2012.

Duan, Q., Sorooshian, S., and Gupta, V. K.: Optimal use of the SCE-UA global optimization method for calibrating watershed models, J. Hydrol., 158, 265–284, https://doi.org/10.1016/0022-1694(94)90057-4, 1994.

Ehret, U., Gupta, H. V., Sivapalan, M., Weijs, S. V., Schymanski, S. J., Blöschl, G., Gelfan, A. N., Harman, C., Kleidon, A., Bogaard, T. A., Wang, D., Wagener, T., Scherer, U., Zehe, E., Bierkens, M. F. P., Di Baldassarre, G., Parajka, J., van Beek, L. P. H., van Griensven, A., Westhoff, M. C., and Winsemius, H. C.: Advancing catchment hydrology to deal with predictions under change, Hydrol. Earth Syst. Sci., 18, 649–671, https://doi.org/10.5194/hess-18-649-2014, 2014.

Fenicia, F., Savenije, H. H. G., Matgen, P., and Pfister, L.: Is the groundwater reservoir linear? Learning from data in hydrological modelling, Hydrol. Earth Syst. Sci., 10, 139–150, https://doi.org/10.5194/hess-10-139-2006, 2006.

Fu, B.: On the calculation of the evaporation from land surface (in Chinese), Sci. Atmos. Sin., 5, 23–31, 1981.

Gao, H., Hrachowitz, M., Schymanski, S. J., Fenicia, F., Sriwongsitanon, N., and Savenije, H. H. G.: Climate controls how ecosystems size the root zone storage capacity at catchment scale, Geophys. Res. Lett., 41, 7916–7923, https://doi.org/10.1002/2014GL061668, 2014.

Gupta, H. V., Kling, H., Yilmaz, K. K., and Martinez, G. F.: Decomposition of the mean squared error and NSE performance criteria: Implications for improving hydrological modelling, J. Hydrol., 377, 80–91, https://doi.org/10.1016/j.jhydrol.2009.08.003, 2009.

Hulsman, P., Bogaard, T. A., and Savenije, H. H. G.: Rainfall-runoff modelling using river-stage time series in the absence of reliable discharge information: a case study in the semi-arid Mara River basin, Hydrol. Earth Syst. Sci., 22, 5081–5095, https://doi.org/10.5194/hess-22-5081-2018, 2018.

Hutley, L. B., Beringer, J., Isaac, P. R., Hacker, J. M., and Cernusak, L. A.: A sub-continental scale living laboratory: Spatial patterns of savanna vegetation over a rainfall gradient in northern Australia, Agr. Forest Meteorol., 151, 1417–1428, https://doi.org/10.1016/j.agrformet.2011.03.002, 2011.

Hutley, L. B., Beringer, J., Fatichi, S., Schymanski, S. J., and Northwood, M.: Gross primary productivity and water use efficiency are increasing in a high rainfall tropical savanna, Glob. Change Biol., 28, 2360–2380, https://doi.org/10.1111/gcb.16012, 2022.

Jeffrey, S. J., Carter, J. O., Moodie, K. B., and Beswick, A. R.: Using spatial interpolation to construct a comprehensive archive of Australian climate data, Environ. Modell. Softw., 16, 309–330, https://doi.org/10.1016/S1364-8152(01)00008-1, 2001.

Keeling, C. D., Piper, S. C., Bacastow, R. B., Wahlen, M., Whorf, T. P., Heimann, M., and Meijer, H. A.: Atmospheric CO2 and 13CO2 Exchange with the Terrestrial Biosphere and Oceans from 1978 to 2000: Observations and Carbon Cycle Implications, in: A History of Atmospheric CO_2 and its effects on Plants, Animals, and Ecosystems, vol. 177 of Ecological Studies, 83–113, Springer Verlag, New York, https://doi.org/10.1007/b138533, edited by: Ehleringer, J. R., Cerling, T. E., and Dearing, M. D., 2005.

Kleidon, A., Renner, M., and Porada, P.: Estimates of the climatological land surface energy and water balance derived from maximum convective power, Hydrol. Earth Syst. Sci., 18, 2201–2218, https://doi.org/10.5194/hess-18-2201-2014, 2014.

Koster, R. D. and Suarez, M. J.: A Simple Framework for Examining the Interannual Variability of Land Surface Moisture Fluxes, J. Climate, 12, 8, 1999.

Levenberg, K.: A method for the solution of certain nonlinear problems in least squares, Q. Appl. Math., 2, 164–168, https://doi.org/10.1090/qam/10666, 1944.

Li, D., Pan, M., Cong, Z., Zhang, L., and Wood, E.: Vegetation control on water and energy balance within the Budyko framework, Water Resour. Res., 49, 969–976, https://doi.org/10.1002/wrcr.20107, 2013.

Mezentsev, V. S.: More on the calculation of average total evaporation, Meteorol. Gidrol, 5, 24–26, 1955.

Mianabadi, A., Coenders-Gerrits, M., Shirazi, P., Ghahraman, B., and Alizadeh, A.: A global Budyko model to partition evaporation into interception and transpiration, Hydrol. Earth Syst. Sci., 23, 4983–5000, https://doi.org/10.5194/hess-23-4983-2019, 2019.

Milly, P. C. D.: Climate, soil water storage, and the average annual water balance, Water Resour. Res., 30, 2143–2156, https://doi.org/10.1029/94WR00586, 1994.

Montanari, A., Young, G., Savenije, H., Hughes, D., Wagener, T., Ren, L., Koutsoyiannis, D., Cudennec, C., Toth, E., Grimaldi, S., Blöschl, G., Sivapalan, M., Beven, K., Gupta, H., Hipsey, M., Schaefli, B., Arheimer, B., Boegh, E., Schymanski, S.,

Di Baldassarre, G., Yu, B., Hubert, P., Huang, Y., Schumann, A., Post, D., Srinivasan, V., Harman, C., Thompson, S., Rogger, M., Viglione, A., McMillan, H., Characklis, G., Pang, Z., and Belyaev, V.: "Panta Rhei–Everything Flows": Change in hydrology and society–The IAHS Scientific Decade 2013–2022, Hydrolog. Sci. J., 58, 1256–1275, https://doi.org/10.1080/02626667.2013.809088, 2013.

Newman, A. J., Clark, M. P., Sampson, K., Wood, A., Hay, L. E., Bock, A., Viger, R. J., Blodgett, D., Brekke, L., Arnold, J. R., Hopson, T., and Duan, Q.: Development of a large-sample watershed-scale hydrometeorological data set for the contiguous USA: data set characteristics and assessment of regional variability in hydrologic model performance, Hydrol. Earth Syst. Sci., 19, 209–223, https://doi.org/10.5194/hess-19-209-2015, 2015.

Nijzink, R.: FLEXsimple, Zenodo, https://doi.org/10.5281/zenodo.7417708, 2022.

Nijzink, R. C and Schymanski, S. J. S.: VOM-v0.6 [code], https://github.com/schymans/VOM/tree/v0.6 (last access: 1 December 2022), 2020.

Nijzink, R. and Schymanski, S.: The role of vegetation optimality in the Budyko framework, Zenodo [data set] and [code], https://doi.org/10.5281/zenodo.7361655, 2022a.

Nijzink, R. C. and Schymanski, S. J.: Technical note: Do different projections matter for the Budyko framework?, Hydrol. Earth Syst. Sci., 26, 4575–4585, https://doi.org/10.5194/hess-26-4575-2022, 2022b.

Nijzink, R. C., Almeida, S., Pechlivanidis, I. G., Capell, R., Gustafssons, D., Arheimer, B., Parajka, J., Freer, J., Han, D., Wagener, T., Nooijen, R. R. P. v., Savenije, H. H. G., and Hrachowitz, M.: Constraining Conceptual Hydrological Models With Multiple Information Sources, Water Resour. Res., 54, 8332–8362, https://doi.org/10.1029/2017WR021895, 2018.

Nijzink, R. C., Beringer, J., Hutley, L. B., and Schymanski, S. J.: Does maximization of net carbon profit enable the prediction of vegetation behaviour in savanna sites along a precipitation gradient?, Hydrol. Earth Syst. Sci., 26, 525–550, https://doi.org/10.5194/hess-26-525-2022, 2022a.

Nijzink, R. C., Beringer, J., Hutley, L. B., and Schymanski, S. J.: Influence of modifications (from AoB2015 to v0.5) in the Vegetation Optimality Model, Geosci. Model Dev., 15, 883–900, https://doi.org/10.5194/gmd-15-883-2022, 2022b.

Ning, T., Li, Z., and Liu, W.: Vegetation dynamics and climate seasonality jointly control the interannual catchment water balance in the Loess Plateau under the Budyko framework, Hydrol. Earth Syst. Sci., 21, 1515–1526, https://doi.org/10.5194/hess-21-1515-2017, 2017.

Ol'Dekop, E.: On evaporation from the surface of river basins, Trans. Meteorol. Obs., 4, 200, 1911.

Oudin, L., Andréassian, V., Lerat, J., and Michel, C.: Has land cover a significant impact on mean annual streamflow? An international assessment using 1508 catchments, J. Hydrol., 357, 303–316, https://doi.org/10.1016/j.jhydrol.2008.05.021, 2008.

Parajka, J., Merz, R., and Blöschl, G.: Uncertainty and multiple objective calibration in regional water balance modelling: case study in 320 Austrian catchments, Hydrolog. Process., 21, 435–446, https://doi.org/10.1002/hyp.6253, 2007.

Perrin, C., Michel, C., and Andréassian, V.: Improvement of a parsimonious model for streamflow simulation, J. Hydrol., 279, 275–289, https://doi.org/10.1016/S0022-1694(03)00225-7, 2003.

Pike, J. G.: The estimation of annual run-off from meteoro-
    logical data in a tropical climate, J. Hydrol., 2, 116–123,
    https://doi.org/10.1016/0022-1694(64)90022-8, 1964.

Porada, P., Kleidon, A., and Schymanski, S. J.: Entropy produc-
    tion of soil hydrological processes and its maximisation, Earth
    Syst. Dynam., 2, 179–190, https://doi.org/10.5194/esd-2-179-
    2011, 2011.

Potter, N. J., Zhang, L., Milly, P. C. D., McMahon, T. A.,
    and Jakeman, A. J.: Effects of rainfall seasonality and
    soil moisture capacity on mean annual water balance for
    Australian catchments, Water Resour. Res., 41, W06007,
    https://doi.org/10.1029/2004WR003697, 2005.

Reaver, N. G. F., Kaplan, D. A., Klammler, H., and Jawitz, J. W.:
    Theoretical and empirical evidence against the Budyko catch-
    ment trajectory conjecture, Hydrol. Earth Syst. Sci., 26, 1507–
    1525, https://doi.org/10.5194/hess-26-1507-2022, 2022.

Renner, M., Seppelt, R., and Bernhofer, C.: Evaluation of water-
    energy balance frameworks to predict the sensitivity of stream-
    flow to climate change, Hydrol. Earth Syst. Sci., 16, 1419–1433,
    https://doi.org/10.5194/hess-16-1419-2012, 2012.

Roderick, M. L. and Farquhar, G. D.: A simple framework for re-
    lating variations in runoff to variations in climatic conditions
    and catchment properties, Water Resour. Res., 47, W00G07,
    https://doi.org/10.1029/2010WR009826, 2011.

Schenk, H. J. and Jackson, R. B.: Rooting depths, lateral root
    spreads and below-ground/above-ground allometries of plants in
    water-limited ecosystems, J. Ecol., 90, 480–494, 2002.

Schreiber, P.: Über die Beziehungen zwischen dem Niederschlag
    und der Wasserführung der Flüsse in Mitteleuropa, Z. Meteor.,
    21, 441–452, 1904.

Schymanski, S. J., Roderick, M. L., Sivapalan, M., Hutley, L. B.,
    and Beringer, J.: A test of the optimality approach to modelling
    canopy properties and CO_2 uptake by natural vegetation, Plant
    Cell Environ., 30, 1586–1598, https://doi.org/10.1111/j.1365-
    3040.2007.01728.x, 2007.

Schymanski, S. J., Sivapalan, M., Roderick, M. L., Beringer, J., and
    Hutley, L. B.: An optimality-based model of the coupled soil
    moisture and root dynamics, Hydrol. Earth Syst. Sci., 12, 913–
    932, https://doi.org/10.5194/hess-12-913-2008, 2008.

Schymanski, S. J., Sivapalan, M., Roderick, M. L., Hut-
    ley, L. B., and Beringer, J.: An optimality-based model
    of the dynamic feedbacks between natural vegetation
    and the water balance, Water Resour. Res., 45, W01412,
    https://doi.org/10.1029/2008WR006841, 2009.

Schymanski, S. J., Roderick, M. L., and Sivapalan, M.: Us-
    ing an optimality model to understand medium and long-
    term responses of vegetation water use to elevated at-
    mospheric CO_2 concentrations, AoB Plants, 7, plv060,
    https://doi.org/10.1093/aobpla/plv060, 2015.

Shao, Q., Traylen, A., and Zhang, L.: Nonparametric method for
    estimating the effects of climatic and catchment characteris-
    tics on mean annual evapotranspiration, Water Resour. Res., 48,
    W03517, https://doi.org/10.1029/2010WR009610, 2012.

Valéry, A., Andréassian, V., and Perrin, C.: 'As simple as pos-
    sible but not simpler': What is useful in a temperature-based
    snow-accounting routine? Part 2 – Sensitivity analysis of the Ce-
    maneige snow accounting routine on 380 catchments, J. Hydrol.,
    517, 1176–1187, https://doi.org/10.1016/j.jhydrol.2014.04.058,
    2014.

Viscarra Rossel, R., Chen, C., Grundy, M., Searle, R., Clifford,
    D., Odgers, N., Holmes, K., Griffin, T., Liddicoat, C., and
    Kidd, D.: Soil and Landscape Grid National Soil Attribute
    Maps – Clay (3" resolution) – Release 1, CSIRO [data set],
    https://doi.org/10.4225/08/546EEE35164BF, 2014a.

Viscarra Rossel, R., Chen, C., Grundy, M., Searle, R., Clifford,
    D., Odgers, N., Holmes, K., Griffin, T., Liddicoat, C., and
    Kidd, D.: Soil and Landscape Grid National Soil Attribute
    Maps - Silt (3" resolution) – Release 1, CSIRO [data set],
    https://doi.org/10.4225/08/546F48D6A6D48, 2014b.

Viscarra Rossel, R., Chen, C., Grundy, M., Searle, R., Clifford,
    D., Odgers, N., Holmes, K., Griffin, T., Liddicoat, C., and
    Kidd, D.: Soil and Landscape Grid National Soil Attribute
    Maps – Sand (3" resolution) – Release 1, CSIRO [data set],
    https://doi.org/10.4225/08/546F29646877E, 2014c.

von Caemmerer, S.: Biochemical Models of Leaf Photosynthe-
    sis, vol. 2 of Techniques in Plant Sciences, CSIRO Publishing,
    Collingwood, https://doi.org/10.1071/9780643103405, 2000.

Wang, D., Zhao, J., Tang, Y., and Sivapalan, M.: A thermody-
    namic interpretation of Budyko and L'vovich formulations of
    annual water balance: Proportionality Hypothesis and maxi-
    mum entropy production, Water Resour. Res., 51, 3007–3016,
    https://doi.org/10.1002/2014WR016857, 2015.

Wang-Erlandsson, L., Bastiaanssen, W. G. M., Gao, H., Jägermeyr,
    J., Senay, G. B., van Dijk, A. I. J. M., Guerschman, J. P., Keys,
    P. W., Gordon, L. J., and Savenije, H. H. G.: Global root zone
    storage capacity from satellite-based evaporation, Hydrol. Earth
    Syst. Sci., 20, 1459–1481, https://doi.org/10.5194/hess-20-1459-
    2016, 2016.

Westhoff, M., Zehe, E., Archambeau, P., and Dewals, B.: Does the
    Budyko curve reflect a maximum-power state of hydrological
    systems? A backward analysis, Hydrol. Earth Syst. Sci., 20, 479–
    486, https://doi.org/10.5194/hess-20-479-2016, 2016.

Whitley, R., Beringer, J., Hutley, L. B., Abramowitz, G., De Kauwe,
    M. G., Duursma, R., Evans, B., Haverd, V., Li, L., Ryu, Y.,
    Smith, B., Wang, Y.-P., Williams, M., and Yu, Q.: A model
    inter-comparison study to examine limiting factors in modelling
    Australian tropical savannas, Biogeosciences, 13, 3245–3265,
    https://doi.org/10.5194/bg-13-3245-2016, 2016.

Williams, C. A., Reichstein, M., Buchmann, N., Baldocchi, D.,
    Beer, C., Schwalm, C., Wohlfahrt, G., Hasler, N., Bernhofer,
    C., Foken, T., Papale, D., Schymanski, S., and Schaefer, K.:
    Climate and vegetation controls on the surface water bal-
    ance: Synthesis of evapotranspiration measured across a global
    network of flux towers, Water Resour. Res., 48, W06523,
    https://doi.org/10.1029/2011WR011586, 2012.

Woods, R.: The relative roles of climate, soil, vegetation
    and topography in determining seasonal and long-term
    catchment dynamics, Adv. Water Resour., 26, 295–309,
    https://doi.org/10.1016/S0309-1708(02)00164-1, 2003.

Yang, D., Sun, F., Liu, Z., Cong, Z., Ni, G., and Lei,
    Z.: Analyzing spatial and temporal variability of annual
    water-energy balance in nonhumid regions of China using
    the Budyko hypothesis, Water Resour. Res., 43, W04426,
    https://doi.org/10.1029/2006WR005224, 2007.

Yang, D., Shao, W., Yeh, P. J.-F., Yang, H., Kanae, S., and Oki, T.:
    Impact of vegetation coverage on regional water balance in the
    nonhumid regions of China, Water Resour. Res., 45, W00A14,
    https://doi.org/10.1029/2008WR006948, 2009.

Yang, H., Yang, D., Lei, Z., and Sun, F.: New analytical derivation of the mean annual water-energy balance equation, Water Resour. Res., 44, W03410, https://doi.org/10.1029/2007WR006135, 2008.

Yang, H., Qi, J., Xu, X., Yang, D., and Lv, H.: The regional variation in climate elasticity and climate contribution to runoff across China, J. Hydrol., 517, 607–616, https://doi.org/10.1016/j.jhydrol.2014.05.062, 2014.

Yokoo, Y., Sivapalan, M., and Oki, T.: Investigating the roles of climate seasonality and landscape characteristics on mean annual and monthly water balances, J. Hydrol., 357, 255–269, https://doi.org/10.1016/j.jhydrol.2008.05.010, 2008.

Zhang, L., Dawes, W. R., and Walker, G. R.: Response of mean annual evapotranspiration to vegetation changes at catchment scale, Water Resour. Res., 37, 701–708, https://doi.org/10.1029/2000WR900325, 2001.

Zhang, L., Hickel, K., Dawes, W. R., Chiew, F. H. S., Western, A. W., and Briggs, P. R.: A rational function approach for estimating mean annual evapotranspiration, Water Resour. Res., 40, W02502, https://doi.org/10.1029/2003WR002710, 2004.

Zhang, S., Yang, H., Yang, D., and Jayawardena, A. W.: Quantifying the effect of vegetation change on the regional water balance within the Budyko framework, Geophys. Res. Lett., 43, 1140–1148, https://doi.org/10.1002/2015GL066952, 2016.